1B.5

WHAT ARE THE FINGER CLOUD IN THE HURRICANE INNER REGION?

Kun Gao[1], Joseph Mouallem[1], Lucas Harris[2]
[1] Princeton University, Princeton, New Jersey
[2] NOAA/Geophysical Fluid Dynamics Laboratory, Princeton, New Jersey

1. OVERVIEW

The inner core region of strong hurricanes or Tropical Cyclones (TCs) harbors complex dynamical features, among which are the fine-scale clouds that exist along the inner-edge of the eyewall, which are characterized by finger-like appearances pointing toward the eye of storm. These features have been observed by aircraft radars in intense hurricanes (Aberson et al. 2006) and are also captured by short-duration Large-Eddy-Simulations of hurricane flow. However, many key aspects of these features still remain unknown, particularly regarding when and why they occur.

This document presents an analysis based on O(100m) grid spacing simulations covering the entire core region of a hurricane and its entire intensification period conducted by the authors. The simulation successfully captured the finger-like clouds, resembling the observed features. Here we document their key characteristics revealed in our simulation and also propose that these features are formed primarily due to the shear instability associated with the tangential wind vertical distribution in the hurricane inner region.

2. MODEL SETUP

We conduct idealized simulation with the GFDL System for High-resolution prediction on Earth-to-Local Domains (SHiELD; Harris et al., 2020), in which the model is initialized with a weak axisymmetric vortex located at the domain center. We use a f-plane assumption and do not prescribe any steering flow. The idealized TC can therefore stay mostly in the domain center as it evolves with time, making it possible to use static nests to cover the hurricane core region.

A two-level nesting strategy (Mouallem et al. 2022) is applied to gradually refine the grid spacing in the TC inner region. The lowest level grid, or the Level 0 grid, is set at 1,600 km x 1,600 km wide with a 2 km uniform horizontal grid spacing. The periodic boundary condition is applied at the East-West and South-North edges of this Level 0 grid. The Level 1 nested grid, which has a grid spacing refined to 500m, is embedded in a 400 km x 400 km area centered around the central point of the Level 0 grid. The Level 2 nested grid, with a 125m grid spacing, is then further embedded within the innermost 100 km x 100 km area of the Level 1 grid.

We use an initial vortex with a maximum wind of approximately 20 m/s at a radius of 125 km, which is centered at the central points of the three grids. The initial environment is set to be spatially uniform. We use a constant Coriolis parameter evaluated at 15N, a fixed uniform sea surface temperature of 302 K. The entire simulation integrates for 4 days, which covers the period from which the TC evolves from a weak vortex to a mature stage.

3. BULK CHARACTERISTICS

Through our visual inspection on the vertical velocity and cloud fields from the Level 1 and Level 2 nested grid solutions, we notice i) alternating updrafts and downdrafts along the inner-edge of the eyewall, and ii) periodic fine-scale cloud features roughly coinciding with the updrafts. These clouds exhibit a distinctive appearance resembling fingers pointing toward the TC eye, and therefore we will refer them to finger clouds hereafter. The finger clouds are about 2-5km wide along the TC azimuthal direction and exist roughly below 3km height. These features merge at approximately Hour 60 of the simulation and occur frequently thereafter.

Our simulated finger clouds seems to resembles the fine-scale cloud features identified in the TC inner-eyewall region by aircraft-based radar observations. **Figure 1** shows a comparison of the radar reflectivity observation collected from hurricane Isabel (2003) when it was at Catergroy-5 status, and the composite radar reflectivity inferred from Level 1 and 2 nest our simulations. Our simulated features, which locate radially inside of the main eyewall, have a similar appearance and spatial scale as the observation features (see circled areas for examples).

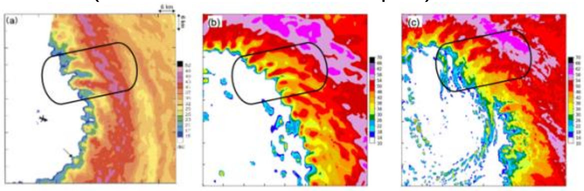

Figure 1. a) Radar reflectivity collected by aircraft from Hurricane Isabel (2003; Figure 5a from Aberson et al. 2006). b) and c) model simulated composite radar reflectivity from the Level 1 and 2 nested grids, respectively.

4. MEAN-EDDY SEPERATION

We propose a regional mean and eddy separation method to facilitate further analysis of eddy structure responsible for the formation of finger clouds. First, we select areas in the TC-centered cylindrical coordinates that contain several eddy features of interest. Then we remap the variables onto the uniform radial-and-azimuthal mesh (with grid spacing consistent with the native model grid spacing). The horizontal winds are projected onto the TC-relative azimuthal and radial components. We then perform moving average along the azimuthal direction in the selected region to obtain the mean flow. This choice recognized that the TC-scale flow has strong variations along the radial direction but less along azimuthal direction. The azimuthal scope for the moving average is set to be 6 degrees. We iterate the averaging twice to ensure a clean separation between the mean flow and eddies. The eddy component is then obtained by subtracting the mean from the total field.

In our following analysis, we focus on the data from Level 1 nested grid. We were able to confirm that the key ideas inferred from this single case can be generalized. **Figure 2** illustrate representative eddy vertical velocity field in Level 1 nested grid obtained via the above method, with key aspects summarized below.

- The eddies are characterized with a classic horizontal roll vortices structure, which are roughly elongated along the TC radial direction. This is the main reason for finger-like appearance of the cloud they caused.
- Their azimuthal and vertical velocity components constitute their overturning circulations.
- Their updrafts peak at 1-2km heights and roughly confined below 4km. The peak eddy vertical velocity shift upward with increasing radius.

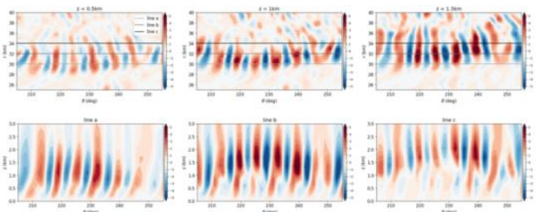

Figure 2. Instantaneous eddy vertical velocity (w') from Level 1 nested grid (dx = 500m). The top panel shows w' on the r-θ plane at three select heights. The lower panel shows cross-sections of w' along three selected arcs (indicated by the three lines in the top panel).

5. PROPOSED FORMATION MECHANISM

Following Nolan (2012), the shear production terms of the eddy kinetic energy (EKE) in a rotating mean flow environment are as follows.

$$\frac{\partial E'}{\partial t} = -\left[\overline{u'v'}\left(\frac{\partial \bar{v}}{\partial r} - \frac{\partial \bar{v}}{\partial r}\right)\right]_{V\_R} - \left[\overline{u'u'}\frac{\partial \bar{u}}{\partial r} + \overline{v'v'}\frac{\bar{u}}{r}\right]_{U\_R} - \left[\overline{u'w'}\frac{\partial \bar{w}}{\partial r}\right]_{W\_R} - \left[\overline{v'w'}\frac{\partial \bar{v}}{\partial z}\right]_{V\_Z} - \left[\overline{u'w'}\frac{\partial \bar{u}}{\partial z}\right]_{U\_Z} - \left[\overline{w'w'}\frac{\partial \bar{w}}{\partial z}\right]_{W\_Z} + \ldots ,$$

where u, v, w are the three wind components in the azimuthal, radial and vertical directions, respectively. The first (last) three terms on the right-hand-side denote the EKE production due to the radial (vertical) shear of the mean tangential, radial and vertical wind components, respectively.

Figure 3 shows the azimuthal-averaged shear-production terms in the above equations for the eddies in Figure 2, which indicates that the V_Z term (i.e., the shear production due to the vertical shear of the tangential wind) is the dominant term, and this term has the largest value at the region where the EKE is strongest. The EKE budget analysis therefore indicates that the eddies are primarily driven by the shear instability associated with the vertical distribution of the tangential wind in the TC inner region.

The strong EKE region indeed overlaps with a strong negative tangential shear layer (**Figure 4**). Interestingly, this negative tangential shear layer coincides with the radial outflow that exists above the BL inflow layer. Such outflow layer exists because of the radially outward force associated with the super-gradient tangential flow in the TC inner region. The negative tangential wind shear layer is presumably formed due to the deceleration of the tangential wind speed caused by the radial outflow, through the conservation of absolute angular momentum.

In summary, we have established a linkage between the formation of eddies with the storm-scale dynamics. Our analysis suggested that the negative tangential shear layer that sit in the radial outflow region can lead to the formation of the eddy features due to the Kelvin-Helmoholtz type of instability. The key characteristics of the eddy features, including their emergence time, frequency, relative radial location, and radial-vertical geometry thus depend on the negative tangential shear layer.

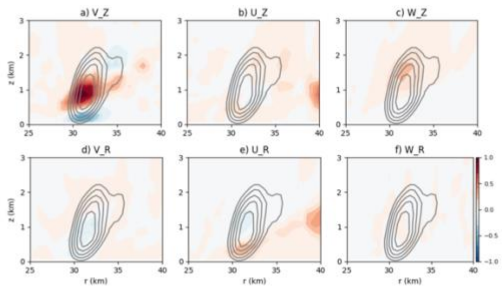

Figure 3. Azimuthal-averaged shear production terms for the eddies in Figure 2. The values are normalized by the maximum value of the V_Z term. The contour lines show the azimuthal-averaged EKE.

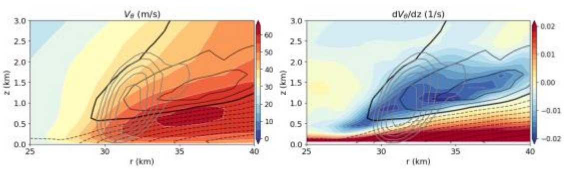

Figure 4. Azimuthal-averaged tangential wind and its vertical shear overlaid with the azimuthal-averaged eddy kinetic energy (gray contours) and the azimuthal-averaged radial wind (black contours; thick line indicate 0 value).

6. REFERENCES

Harris, L., et al., 2020, GFDL SHiELD: A unified system for weather-to-seasonal prediction. Journal of Advances in Modeling Earth Systems, 12, e2020MS002 223.

Mouallem, J., L. Harris, and R. Benson, 2022: Multiple same-level and telescoping nesting in GFDL's dynamical core, GMD, 15 (11), 4355–4371, 2022.

Aberson, S. D., M. T. Montgomery, M. Bell, and M. Black, 2006: Hurricane Isabel (2003): New insights into the physics of intense storms. Part II: Extreme localized wind. Bull. Amer. Meteor. Soc., 87, 1349–1354.

Nolan, D. S., 2012: Three-dimensional instabilities in tornado-like vortices with secondary circulations. J. Fluid Mech., 711, 61–100.